Self-consistent numerical modeling of radiatively damped Lorentz oscillators

Ellen Schelew
Department of Physics and Astronomy, University of British Columbia, Vancouver British Columbia, Canada V6T 1Z1 and Lumerical Solutions, Inc., Vancouver British Columbia, Canada V6E 2M6

Rong-Chun Ge and Stephen Hughes
Department of Physics, Queen's University, Kingston Ontario, Canada K7L 3N6

James Pond
Lumerical Solutions, Inc., Vancouver British Columbia, Canada V6E 2M6

Jeff F. Young*
Department of Physics and Astronomy, University of British Columbia, Vancouver British Columbia, Canada V6T 1Z1
(Received 4 October 2016; revised manuscript received 4 April 2017; published 30 June 2017)

Recent progress towards realizing quantum emitters (QEs) suitable for integration in quantum information networks stimulates the demand for a self-consistent numerical approach to describe scattering of radiatively limited QEs in complex dielectric environments. As the QE response has to be characterized without the use of phenomenological damping parameters, the divergent nature of the pointlike emitter's in-phase self-field has to be carefully dealt with to avoid unphysical frequency shifts. Here we provide a solution to this problem and show two ways to obtain accurate results in the weak excitation limit using finite-difference time-domain algorithms. One of these approaches lays important groundwork needed for future simulations of nonlinear QE networks. The solution for dealing with the frequency shift reveals that dynamical contributions to the resonant depolarization field of arbitrarily small dielectric objects make crucial contributions to the net dipole moment induced by an external field when radiative scattering is the only source of damping.

DOI: 10.1103/PhysRevA.95.063853

I. INTRODUCTION

Recent interest in using photons to mediate the exchange of quantum information between quantum emitters (QEs; impurity states within solids, individual atoms or molecules, artificial quantum dots, etc.) makes relevant the issue of how to numerically treat the interaction of a collection of such quantum emitters in a complex dielectric environment ($\epsilon_B(\mathbf{r})$; dielectric, metallic, or hybrid cavity structure typically coupled in turn to a continuum, such as vacuum) [1–6]. If the QE's electronic response is damped primarily by nonradiative processes such as pure dephasing, then it is justified to use a relatively straightforward form of the Maxwell-Bloch equations in which the electronic response is phenomenologically damped [7,8]. This has allowed researchers to study light-matter interactions in nonlinear materials without recourse to rotating-wave or slowly-varying-envelope approximations, leading to the predictions of new phenomena such as the dynamic nonlinear skin effect [9] and carrier-wave Rabi flopping [10]. However, QEs whose response is dictated by nonradiative dissipative processes are of limited use for quantum information applications, so to properly deal with systems damped primarily by radiative decay, the electric field entering the Maxwell-Bloch analysis has to self-consistently provide the coherent radiative contribution to the damping of the QEs [11]. It is the component of the field at the QE that is 90 degrees out of phase with the QE's dipole response, the quadrature field, that generates this "radiation reaction," and this component is typically numerically well-behaved. The component of the field at the QE that is in phase with the induced dipole oscillation is also important, since it in general leads to dielectric-environment-induced shifts of the QE's resonant frequency. However, numerically there is a divergent in-phase contribution to the field at the location of the QE (the ideal point dipole has an infinite in-phase self-field), and care must be taken to remove this divergent self-field from the simulation [11,12].

One approach to solving this problem is to formulate it in terms of photon Green functions (GFs) and/or a quantum master equation. In a complex scenario with many QEs in a non-trivial dielectric environment, the QEs are typically treated as pointlike two-level systems (TLSs) at different locations with respect to cavities that support quasinormal with finite lifetimes due to coupling to the continuum of electromagnetic modes and outgoing boundary conditions [13,14]. The actual quasinormal modes and their impact on the decay rate and natural frequency of each QE almost always needs to be numerically evaluated by finding the photon GF at the location of each QE [15]. Finite-difference time-domain (FDTD) simulators, such as provided by Lumerical Solutions Inc., offer one way to accurately determine these GFs. For each QE location $\mathbf{r}_0^i$, a "point dipole" located at $\mathbf{r}_0^i$ is driven with fixed amplitude, first in the nonuniform dielectric background environment specified by $\epsilon_B(\mathbf{r})$ (that does not include any of the QEs), and then in a globally uniform version of the dielectric background medium at $\mathbf{r}_0^i$. The real and imaginary parts of the field at the QE location give the corresponding nonuniform and uniform background dielectric GFs, and the real part of the uniform GF is subtracted from the real part

*young@phas.ubc.ca

of the nonuniform GF, yielding a total GF that removes the divergent real part of the dipole's self-field. The Purcell factor for each individual QE is calculated by taking the ratio of the imaginary parts of the nonuniform and uniform background dielectric GFs. Self-consistency of the response of the entire coupled system to some external electromagnetic excitation then requires careful formulation of the coupling equations, along with these GFs.

If one is using a numerical solver, it is interesting to ask: Is there a way to perform just one numerical simulation that self-consistently couples all QEs and the dielectric environment when solving for its response to an electromagnetic excitation? While we have not yet answered this question for arbitrarily strong excitation fields, we have identified and solved a number of practical issues in the weak excitation limit that are essential for future work that will extend this to the high-excitation regime. This paper describes two different methods for self-consistently and accurately capturing the damping associated with radiation reaction, and the resonant frequency shifts introduced by scattering from the dielectric environment, without using any phenomenological damping parameters. In these approaches, the addition of phenomenological radiative damping terms would be erroneous, as radiative damping naturally arises through the FDTD method. The accuracy is demonstrated in a weak excitation limit where, to a good approximation, the QE behaves as a Lorentz oscillator (LO) with a renormalized resonant frequency and radiative decay rate.

While we use an FDTD-based numerical approach to illustrate the scheme, many of the fundamental issues are generic to any numerical engine that solves the Maxwell equations on some cubic three-dimensional (3D) mesh. The task is essentially to define some dielectric object on a 3D mesh that faithfully represents the LO response to the field produced at that LO by (i) external sources, (ii) all other polarizable elements in the environment, and (iii) the quadrature component of the LO's self-field. The challenge lies in deriving an effective dielectric function for this object that accurately and passively removes the effect of the divergent component of that self-field.

The remainder of the manuscript is organized as follows. Section II A first identifies the target pointlike LO response function in general terms appropriate to an arbitrarily complex dielectric environment. This polarizability, $\alpha(\omega)$, is proportional to the ratio of the dipole moment induced in the pointlike dipole to the external field present at the dipole, omitting all self-fields, and is parametrized by the LO's resonant frequency and dipole transition moment.

In Sec. II B, the QE is modeled as a deep-sub-wavelength size sphere and its dielectric function is derived. The bulk susceptibility model used to define the dielectric function includes various dynamical contributions to the depolarization field. By dividing the total dipole moment of the sphere by the external driving field, and then equating this to $\alpha(\omega)$ (with the same proportionality constant), an explicit form of the dielectric function required to mimic the pointlike dipole is obtained, which depends on the QE properties and the sphere radius. This effective, purely real, sphere-radius-dependent dielectric function that contains no phenomenological damping terms accurately mimics the pointlike dipole response of an isolated sphere in vacuum, including radiation reaction effects. This is demonstrated by evaluating the response of spheres with sizes ranging from 5 to 30 nm using an exact Mie scattering calculation. The crucial, and somewhat unintuitive role played by the dynamical contributions to the depolarization field are clearly identified. The remainder of Sec. II B demonstrates how conventional FDTD simulations of the same spheres fail to provide reliable results, even when the bulk sphere is described by up to 33,000 Yee cells. It is argued that these results might be expected based on the insight gained from the Mie calculations.

Section II C describes the most important practical result of this work, that with only a slight modification, the same effective dielectric function can be used to define a "dielectric object" *on a single Yee cell*, that again faithfully mimics the desired pointlike dipole response. Some insights regarding this somewhat surprising result are offered, aided by an alternate approach to numerically solving the same problem in FDTD. This alternate approach, which offers a much more flexible means of extending such simulations to higher excitation levels, is described in Sec. II D.

Section III offers a simple example application of this numerical scheme where the resonant frequency shift and modified spontaneous lifetime of a LO in the vicinity of a metal half-space is demonstrated.

II. SELF-CONSISTENT DIELECTRIC RESPONSE FUNCTION OF AN IDEAL LORENTZ OSCILLATOR IN A COMPLEX DIELECTRIC ENVIRONMENT

A. Target point-dipole response

The overall objective is to define a dielectric object on a 3D numerical mesh that responds in an electromagnetic environment exactly as an ideal point-dipole responds. For a purely radiatively damped pointlike LO located at a position $\mathbf{r}_0$ in a complex isotropic dielectric environment defined by relative permittivity $\epsilon_{\mathrm{B}}(\mathbf{r})$, the linear response of the LO dipole moment $\mathbf{p}(\mathbf{r}_0,\omega) = |\mathbf{p}(\mathbf{r}_0,\omega)|\mathbf{n}$, to a field $\widetilde{\mathbf{E}}_{\mathrm{B}}(\mathbf{r}_0,\omega)$ produced at the dipole location $\mathbf{r}_0$ by some external field incident on $\epsilon_{\mathrm{B}}(\mathbf{r})$, is given by $\mathbf{p}(\mathbf{r}_0,\omega) = \epsilon_0\alpha(\omega)\widetilde{\mathbf{E}}_{\mathrm{B}}(\mathbf{r}_0,\omega)$, with polarizability

$$\alpha(\omega) = \frac{2\omega_0\mu^2\epsilon_0^{-1}\hbar^{-1}}{\omega_0^2 - \omega^2 - 2\omega_0\mu^2\hbar^{-1}(\mathbf{n}\cdot\mathbf{G}(\mathbf{r}_0,\mathbf{r}_0,\omega)\cdot\mathbf{n})}, \quad (1)$$

where ω_0 is the LO resonance frequency, and μ is the off-diagonal dipole transition matrix element for an isotropic dipole. In this discussion, electric fields marked with a tilde (e.g., $\widetilde{\mathbf{E}}$) are complex amplitudes, such that the time-dependent fields are $\mathbf{E}(t) = \mathrm{Re}[\widetilde{\mathbf{E}}(\mathbf{r_0},\omega)\exp(-i\omega t)]$. For reference, a summary of the electric fields discussed here and in the following sections is provided in Appendix A.

The GF tensor, $\mathbf{G}(\mathbf{r},\mathbf{r}_0,\omega)$, solves the wave equation,

$$\nabla\times\nabla\times\mathbf{G}(\mathbf{r},\mathbf{r}_0,\omega) - \epsilon_{\mathrm{B}}(\mathbf{r},\omega)\frac{\omega^2}{c^2}\mathbf{G}(\mathbf{r},\mathbf{r}_0,\omega) = \frac{\omega^2}{\epsilon_0 c^2}\delta(\mathbf{r}-\mathbf{r}_0)\mathbf{1}, \quad (2)$$

where $\mathbf{1}$ is the identity tensor. The electric field generated at the location of a fixed-amplitude oscillating point dipole is then $\widetilde{\mathbf{E}}_{\mathrm{p}}(\mathbf{r}_0,\omega) = \mathbf{G}(\mathbf{r}_0,\mathbf{r}_0,\omega)\cdot\mathbf{p}(\mathbf{r}_0,\omega)$. The GF includes contributions from the self-field of the dipole due to $\mathbf{p}(\mathbf{r}_0,\omega)$, $\mathbf{G}_0(\mathbf{r}_0,\mathbf{r}_0,\omega)$ and from the scattered field

$\mathbf{G}_{\rm scatt}(\mathbf{r}_0,\mathbf{r}_0,\omega)$. The response function in (1) will not, in general, have a Lorentzian line shape, but in many practical circumstances, including the examples treated below, it is Lorentzian to a good approximation. In some simple geometries the GF can be calculated analytically, but usually it must be obtained numerically. So long as the dipole is located in a region where $\epsilon_{\rm B}$ has no imaginary part, then analytically, $\mathrm{Re}[\mathbf{G}_0(\mathbf{r}_0,\mathbf{r}_0,\omega)]$ is infinite, while $\mathrm{Im}[\mathbf{G}_0(\mathbf{r}_0,\mathbf{r}_0,\omega)]$ is well behaved (and is directly proportional to the radiative damping rate of the dipole if it were in a uniform version of the dielectric medium at $\mathbf{r}_0$). Depending on the numerical approach taken, $\mathrm{Im}[\mathbf{G}_0(\mathbf{r}_0,\mathbf{r}_0,\omega)]$ will readily converge for appropriate parameters used in a meshing scheme, but $\mathrm{Re}[\mathbf{G}_0(\mathbf{r}_0,\mathbf{r}_0,\omega)]$ will take on some large (grid-size dependent) value that does not converge. The real and imaginary parts of $\mathbf{G}_{\rm scatt}(\mathbf{r}_0,\mathbf{r}_0,\omega)$ are nondivergent (analytically and numerically), so the total $\mathrm{Im}[\mathbf{G}(\mathbf{r}_0,\mathbf{r}_0,\omega)]$ then is directly proportional to the overall radiative damping rate that enters the response function $\alpha(\omega)$. The radiative damping rate, $\Gamma = 2\mu^2\hbar^{-1}\mathbf{n}\cdot\mathrm{Im}[\mathbf{G}(\mathbf{r}_0,\mathbf{r}_0,\omega)]\cdot\mathbf{n}$, is consistent with that found for a two-level atom using Fermi's golden rule [16]. Once the divergent self-field contribution, $\mathrm{Re}[\mathbf{G}_0(\mathbf{r}_0,\mathbf{r}_0,\omega)]$, is either ignored or subtracted from the numerically calculated total field, $\mathrm{Re}[\mathbf{G}_{\rm scatt}(\mathbf{r}_0,\mathbf{r}_0,\omega)]$ then causes a shift in the resonant frequency of the response function $\alpha(\omega)$.

The complete solution of the scattering problem defined when a specified external field $\mathbf{E}_{\rm ext}(t)$ is incident on the region defined by $\epsilon(\mathbf{r}) = \epsilon_0\epsilon_{\rm r}(\mathbf{r})$, *including* a QE defined by a resonant frequency ω_0 and a dipole strength μ, located at position $\mathbf{r}_0$, then requires that the field generated by the QE be included self-consistently. Finite-difference time-domain solvers offer a powerful means of evaluating scattering problems defined by an external field incident on a region defined by some function $\epsilon_{\rm r}(\mathbf{r})$, or more generally, $\epsilon_{\rm r}(\mathbf{r},\omega)$. In most instances, the electric field that the FDTD solver evaluates is the *macroscopic field* $\widetilde{\mathbf{E}}(\mathbf{r},\omega)$ that is related to the macroscopic polarization density $\mathbf{P}(\mathbf{r},\omega)$ as $\mathbf{P}(\mathbf{r},\omega) = \epsilon_0\chi(\mathbf{r},\omega)\widetilde{\mathbf{E}}(\mathbf{r},\omega)$, where $\chi(\mathbf{r},\omega) = \epsilon_{\rm r}(\mathbf{r},\omega) - 1$, which requires that the mesh size on which the fields and materials are defined must be significantly finer than the dimensions over which $\epsilon_{\rm r}(\mathbf{r},\omega)$ varies appreciably. Within that paradigm, how can the response function of a pointlike LO be used to define a dielectric object characterized by a small, localized bulk susceptibility $\chi_{\rm LO}(\mathbf{r},\omega)$, that faithfully represents the LO behavior in a FDTD simulation that includes $\epsilon_{\rm B}(\mathbf{r},\omega)$, such that $\epsilon_{\rm r}(\mathbf{r},\omega) = 1 + \chi_{\rm B}(\mathbf{r},\omega) + \chi_{\rm LO}(\mathbf{r},\omega)$?

B. Rendering the LO as a bulk dielectric sphere

Consider a sphere of radius R centered at a point $\mathbf{r}_0$, with a volume V much much smaller than λ^3, as small as numerical limits on the mesh size allow. The sphere resides within some background dielectric environment $\epsilon_{\rm B}(\mathbf{r})$ that varies little over R near $\mathbf{r}_0$. The total field generated inside the sphere $\widetilde{\mathbf{E}}_{\rm tot}(\mathbf{r})$, in the presence of an applied field $\widetilde{\mathbf{E}}_{\rm B}(\mathbf{r})$, that consists of some external field that scatters off of the background dielectric texture $\epsilon_{\rm B}(\mathbf{r})$, can be expressed as

$$\widetilde{\mathbf{E}}_{\rm tot}(\mathbf{r}) \simeq \widetilde{\mathbf{E}}_{\rm B}(\mathbf{r_0}) + \widetilde{\mathbf{E}}_{\rm LO}(\mathbf{r}) + \widetilde{\mathbf{E}}_{\rm scatt}(\mathbf{r_0}), \tag{3}$$

where $\widetilde{\mathbf{E}}_{\rm LO}$ is the electric field inside the sphere generated by the incremental polarization density associated with the LO, $\mathbf{P}_{\rm LO}(\mathbf{r})$, and $\widetilde{\mathbf{E}}_{\rm scatt}$ is the field generated by the incremental polarization density that is scattered back to the dipole from texture in $\epsilon_{\rm B}(\mathbf{r})$. Here it is assumed that both the externally generated field and this incremental scattered field vary little over the extent of the sphere.

As shown below, in order for the sphere's response to mimic that of a pointlike dipole, it is crucial to carefully evaluate $\widetilde{\mathbf{E}}_{\rm LO}(\mathbf{r})$, which is given by

$$\begin{aligned}\widetilde{\mathbf{E}}_{\rm LO}(\mathbf{r}) &= \int_V \mathbf{G}_0(\mathbf{r},\mathbf{r}')\cdot\mathbf{P}_{\rm LO}(\mathbf{r}')d\mathbf{r}' \\ &= -\frac{1}{3\epsilon_0\epsilon_{\rm B}(\mathbf{r}_0)}\mathbf{P}_{\rm LO}(\mathbf{r}) + \int_{V_\sigma}\mathbf{G}_0(\mathbf{r},\mathbf{r}')\cdot\mathbf{P}_{\rm LO}(\mathbf{r}')d\mathbf{r}',\end{aligned} \tag{4}$$

where the first integral is over the entire volume of the sphere V and the second is over volume V_σ, which is the same as V but excludes an infinitely small region around $\mathbf{r} = \mathbf{r}'$. The uniform medium GF is given by [16]

$$\begin{aligned}\mathbf{G}_0(\mathbf{r},\mathbf{r}') = \frac{e^{ik_{\rm B}\rho}}{4\pi\epsilon_0\epsilon_{\rm B}}\Bigg(&\left[\frac{(k_{\rm B})^2}{\rho} + \frac{ik_{\rm B}}{\rho^2} - \frac{1}{\rho^3}\right]\mathbf{1} \\ &- \left[\frac{(k_{\rm B})^2}{\rho} + \frac{3ik_{\rm B}}{\rho^2} - \frac{3}{\rho^3}\right]\frac{\boldsymbol{\rho}\otimes\boldsymbol{\rho}}{\rho^2}\Bigg),\end{aligned} \tag{5}$$

where $\boldsymbol{\rho} = \mathbf{r} - \mathbf{r}'$, $\rho = |\boldsymbol{\rho}|$, $k_{\rm B} = \frac{\omega}{c}\sqrt{\epsilon_{\rm B}}$, and $\otimes$ is the outer product. If only the leading order real ($\sim 1/\rho^3$) and imaginary ($\sim k_{\rm B}/\rho^2$) contributions to $\mathbf{G}_0(\mathbf{r},\mathbf{r}')$ are retained after expanding the exponential, one obtains a solution for $\widetilde{\mathbf{E}}_{\rm LO}(\mathbf{r})$ from Eq. (4) that has constant real and imaginary components throughout the sphere. The real part consists only of the static dipole result for a sphere, while the imaginary part corresponds to the field responsible for radiation damping, such that the total field is

$$\begin{aligned}\widetilde{\mathbf{E}}_{\rm tot}(\mathbf{r}) = \widetilde{\mathbf{E}}_{\rm tot}(\mathbf{r_0}) &\simeq \widetilde{\mathbf{E}}_{\rm B}(\mathbf{r_0}) + \widetilde{\mathbf{E}}_{\rm LO}(\mathbf{r_0}) + \widetilde{\mathbf{E}}_{\rm scatt}(\mathbf{r_0}) \simeq \widetilde{\mathbf{E}}_{\rm B}(\mathbf{r_0}) \\ &- \frac{1}{3\epsilon_0\epsilon_{\rm B}(r_0)}\mathbf{P}_{\rm LO}(\mathbf{r_0}) + \frac{i\omega^3\sqrt{\epsilon_{\rm B}(\mathbf{r}_0)}}{6\pi\epsilon_0 c^3}\mathbf{P}_{\rm LO}(\mathbf{r_0})V \\ &+ \mathbf{G}_{\rm scatt}(\omega)\cdot\mathbf{P}_{\rm LO}(\mathbf{r_0})V,\end{aligned} \tag{6}$$

for all $\mathbf{r}$ inside the sphere. In the above, $\widetilde{\mathbf{E}}_{\rm scatt}$ has been expressed in terms of the scattering GF, $\mathbf{G}_{\rm scatt}(\mathbf{r}_0,\mathbf{r}_0)$ (final term on the right-hand side).

The differential polarization density due to the LO is given by

$$\mathbf{P}_{\rm LO}(\mathbf{r}) = \epsilon_0\chi_{\rm LO}\widetilde{\mathbf{E}}_{\rm tot}(\mathbf{r}), \tag{7}$$

where $\chi_{\rm LO} = \epsilon_{\rm r}(\mathbf{r}_0) - \epsilon_{\rm B}(\mathbf{r}_0)$. It follows that

$$\widetilde{\mathbf{E}}_{\rm tot} = \frac{\widetilde{\mathbf{E}}_{\rm B}}{1 + \frac{\epsilon_{\rm r}-\epsilon_{\rm B}}{3\epsilon_{\rm B}} - \left(i\frac{\omega^3\sqrt{\epsilon_{\rm B}}}{6\pi\epsilon_0 c^3} + \mathbf{n}\cdot\mathbf{G}_{\rm scatt}\cdot\mathbf{n}\right)\epsilon_0(\epsilon_{\rm r} - \epsilon_{\rm B})V}, \tag{8}$$

where the common position argument has been suppressed to simplify notation, including in the dielectric functions, i.e., $\epsilon_{\rm r}(\mathbf{r}_0)$ and $\epsilon_{\rm B}(\mathbf{r}_0)$ are written as $\epsilon_{\rm r}$ and $\epsilon_{\rm B}$. In order for this sphere to mimic a purely radiatively damped pointlike dipole (LO), consider the incremental dipole moment of the sphere

(with total relative dielectric constant, ϵ_r):

$$\mathbf{p}_{\rm LO} = V\mathbf{P}_{\rm LO} \tag{9a}$$

$$= \frac{\widetilde{\mathbf{E}}_{\rm B}}{\frac{2\epsilon_{\rm B}+\epsilon_r}{3\epsilon_0\epsilon_{\rm B}(\epsilon_r-\epsilon_{\rm B})V} - \left(i\frac{\omega^3\sqrt{\epsilon_{\rm B}}}{6\pi\epsilon_0 c^3} + \mathbf{n}\cdot\mathbf{G}_{\rm scatt}(\omega)\cdot\mathbf{n}\right)} \tag{9b}$$

$$\equiv \epsilon_0\alpha\widetilde{\mathbf{E}}_{\rm B}. \tag{9c}$$

The point-dipole response function at point $\mathbf{r}_0$ in the environment defined by $\epsilon_{\rm B}(\mathbf{r})$ is, from Eq. (1) with $\mathrm{Im}[G_0(\mathbf{r}_0,\mathbf{r}_0,\omega)] = \omega^3\sqrt{\epsilon_{\rm B}(\mathbf{r}_0,\omega)}/(6\pi\epsilon_0 c^3)$ and $\mathrm{Re}[G_0(\mathbf{r}_0,\mathbf{r}_0,\omega)]$ removed,

$$\alpha(\omega) = \frac{2\omega_0\mu^2\epsilon_0^{-1}\hbar^{-1}}{\omega_0^2-\omega^2-2\omega_0\mu^2\hbar^{-1}\left(i\frac{\omega^3\sqrt{\epsilon_{\rm B}}}{6\pi\epsilon_0 c^3}+\mathbf{n}\cdot\mathbf{G}_{\rm scatt}(\omega)\cdot\mathbf{n}\right)}, \tag{10}$$

so when the macroscopic dielectric sphere's response is equated to that of a radiatively damped point dipole, the following expression involving the dielectric function results:

$$\frac{\epsilon_r/\epsilon_{\rm B}-1}{\epsilon_r/\epsilon_{\rm B}+2} = \frac{1}{3V\epsilon_{\rm B}}\alpha_0(\omega), \tag{11}$$

where

$$\alpha_0(\omega) \equiv \frac{2\omega_0\mu^2\epsilon_0^{-1}\hbar^{-1}}{\omega_0^2-\omega^2} \tag{12}$$

is the bare polarizability for a point LO dipole, where $\mathbf{p}(\mathbf{r}_0,\omega) = \epsilon_0\alpha_0(\omega)\widetilde{\mathbf{E}}_{\rm tot}(\mathbf{r}_0,\omega)$, so

$$\epsilon_r = \epsilon_{\rm B} + \frac{\alpha_0(\omega)/V}{1-\alpha_0(\omega)/(3\epsilon_{\rm B}V)}. \tag{13}$$

It is interesting, given the distinct differences in their derivations, that in vacuum ($\epsilon_{\rm B}=1$), this is exactly what one would obtain using the well-known Lorentz-Lorenz relation to determine the effective dielectric constant of a collection of pointlike, radiatively damped dipoles, with a density of $1/V$. The Lorentz-Lorenz relation has previously been considered in self-consistent implementations of the Maxwell-Bloch equations as applied to macroscopic media [17–19].

To assess the extent to which this derivation achieves the goal of accurately mimicking the point-dipole response function, the fields generated by exciting a uniform sphere with dielectric function defined by Eq. (13) are calculated using "exact" Mie scattering formulas as a function of sphere radius R [20,21]. Figure 1(a) shows the dielectric function in Eq. (13) as a function of ω for a sphere with $\omega_0 = 3.55\times10^{15}$ rad/s, $\mu = 690$ D, $R = 10$ nm, and $V = 4\pi R^3/3$.[1] The spectrum of the decaying fields generated by the impulsively excited sphere for several R ranging from 5 to 30 nm are plotted in Fig. 1(b). While the linewidth is within 3% of that expected due to radiation reaction for all R, the resonant frequency diverges from its nominal value as $1/R$. The magnitudes of the peak frequency shifts are plotted in Fig. 1(c), with

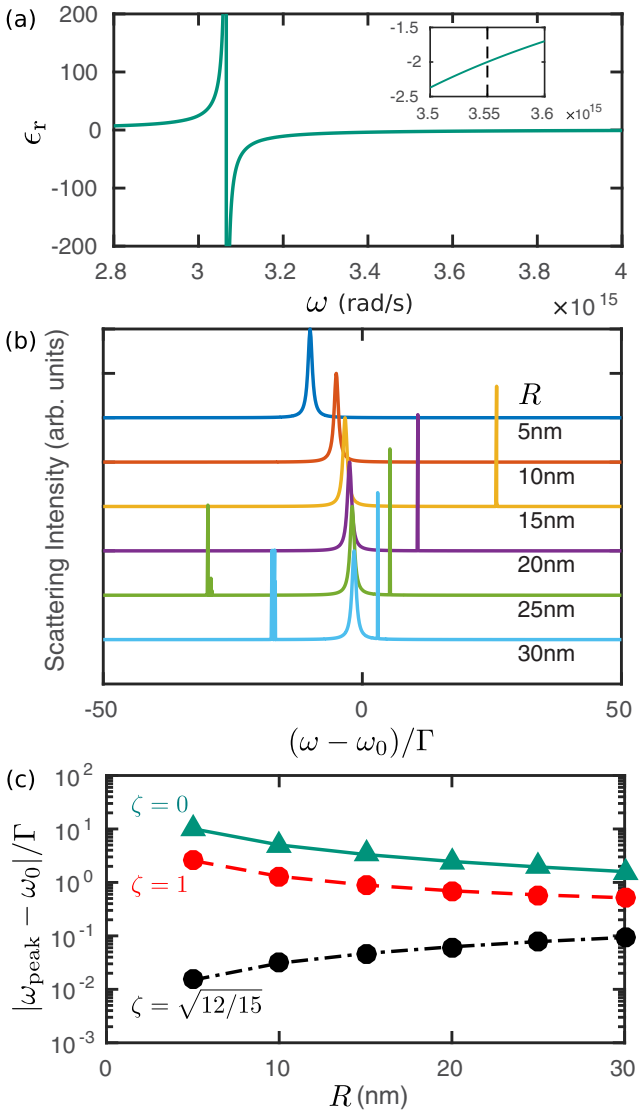

FIG. 1. (a) Dielectric function for a sphere of LO material given by Eq. (13), with $\omega_0 = 3.55\times10^{15}$ rad/s, $\mu = 690$ D, $\Gamma = 1\times10^{12}$ rad/s, $R = 10$ nm, and $V = 4\pi R^3/3$. The inset shows the dielectric function near ω_0, marked with a dashed line. (b) Mie scattering intensity spectra generated by sphere LO materials described by the dielectric function in (a), but for sphere radii ranging between 5 and 30 nm, as labeled on the plot. The broadest peaks in each spectra are the dipole-resonance peaks. (c) Magnitudes of the resonant frequency shifts normalized by Γ, versus the sphere radii in (b). The data connected by solid, dashed, and dash-dotted lines are calculated for spheres with LO material permittivities given by Eq. (16), where $\zeta = 0, 1$ and $\sqrt{12/15}$, respectively. Triangle and circles markers indicate negative and positive shifts, respectively. Note the Γ normalization applied to the shift is appropriate because the absolute frequency shifts and the linewidths are derived from the second and third lines, respectively, of Eq. (6), using a common scale factor proportional to the assumed dipole transition moment squared [see Eq. (17)].

triangle markers connected by a solid line. Triangle markers are used to indicate that the shifts are negative, as seen in Fig. 1(b). The reason for this problematic shift can be traced to the inclusion of only the lowest order ($\sim1/\rho^3$) term in

[1]The large dipole moment strength was chosen here in order to resolve the resonant peak of interest in simulations of a sphere (discussed at the end of this section) using a practical run-time.

the real part of $\mathbf{G}_0(\mathbf{r},\mathbf{r}')$. While only the lowest-order term in the imaginary component of $\mathbf{G}_0(\mathbf{r},\mathbf{r}')$ is adequate to describe radiative damping effects via the out-of-phase term in the sphere's self-field, it is necessary to include higher-order, dynamic terms in the in-phase component of $\mathbf{G}_0(\mathbf{r},\mathbf{r}')$ in order to remove the $1/R$ divergence of the resonant frequency shift illustrated in Fig. 1(c).

When the next-higher-order term ($\sim k_B^2/\rho$) in the real part of $\mathbf{G}_0(\mathbf{r},\mathbf{r}')$ is included, the integral in Eq. (4) results in a contribution to $\widetilde{\mathbf{E}}_{LO}(\mathbf{r})$ that varies over the sphere, even if $\mathbf{P}_{LO}(\mathbf{r})$ is approximated as a constant. A relatively simple expression for $\widetilde{\mathbf{E}}_{LO}(\mathbf{r})$ can be retained if the spatial variation is neglected, and the higher-order contribution is only evaluated at $\mathbf{r} = \mathbf{r_0}$. This leads to an improved expression for $\widetilde{\mathbf{E}}_{tot}(\mathbf{r_0})$ [cf. Eq. (6)]:

$$\widetilde{\mathbf{E}}_{tot}(\mathbf{r}) = \widetilde{\mathbf{E}}_{tot}(\mathbf{r_0}) \simeq \widetilde{\mathbf{E}}_B(\mathbf{r_0}) + \widetilde{\mathbf{E}}_{LO}(\mathbf{r_0}) + \widetilde{\mathbf{E}}_{scatt}(\mathbf{r_0}) \simeq \widetilde{\mathbf{E}}_B(\mathbf{r}_0) - \frac{1}{3\epsilon_0\epsilon_B(r_0)}\mathbf{P}_{LO}(\mathbf{r_0})[1-(k_B R)^2] + \frac{i\omega^3\sqrt{\epsilon_B(\mathbf{r}_0)}}{6\pi\epsilon_0 c^3}\mathbf{P}_{LO}(\mathbf{r_0})V + \mathbf{G}_{scatt}(\omega)\cdot\mathbf{P}_{LO}(\mathbf{r_0})V. \quad (14)$$

The dashed line in Fig. 1(c) shows that by including this higher-order term, the divergent resonant frequency shift is dramatically reduced while the linewidth remains accurate. To remove the remaining shift of the resonant frequency, it is necessary to include the nonuniform nature of the field within the sphere when evaluating Eq. (4). This is discussed in Appendix B, but the result is the addition of one more term in Eq. (14) that also behaves as k_B/ρ^2, such that when both k_B/ρ^2 terms are taken together, the effective result is setting $R \to \zeta R$ in Eq. (14), where $\zeta = \sqrt{12/15} \simeq 0.8944$ [22,23]. When this relationship is used with Eqs. (7) and (9c) to define the desired bulk dielectric function to assign to the sphere, one gets

$$\frac{\epsilon_r/\epsilon_B - 1}{\epsilon_r/\epsilon_B + 2} = \left[\left(\frac{1}{3V\epsilon_B}\alpha_0(\omega)\right)^{-1} + (k_B\zeta R)^2\right]^{-1}, \quad (15)$$

such that

$$\epsilon_r = \epsilon_B + \frac{\alpha_0(\omega)/V}{1-\alpha_0(\omega)[1-(k_B\zeta R)^2]/(3\epsilon_B V)}, \quad (16)$$

or approximately (when $\omega \approx \omega_0$),

$$\epsilon_r \simeq \epsilon_B + \frac{\mu^2/(\epsilon_0\hbar V)}{\omega_0 - \omega - [1/V - 3(k_B\zeta)^2/(4\pi R)]\mu^2/(3\epsilon_B\epsilon_0\hbar)}. \quad (17)$$

The dash-dotted line in Fig. 1(c) shows that Eq. (16) achieves the desired result: when this lossless, radius-dependent dielectric function is used to describe the bulk properties of a deep subwavelength diameter sphere, the sphere mimics the decay of a pointlike LO with the associated resonant frequency and dipole transition matrix element, faithfully capturing the radiation reaction physics self-consistently without introducing any phenomenological damping parameters.

The second form of ϵ_r in Eq. (17) makes clear why, in this problem, it is necessary to include dynamical effects when evaluating the depolarization field, even in the limit of arbitrarily small spheres. The frequency shift of the LO associated with the divergent component of the self-field contains two terms: $[1/V - 3(k_B\zeta)^2/(4\pi R)]\mu^2/(3\epsilon_B\epsilon_0\hbar)$. The static depolarization contribution diverges as $1/V$, but the lowest-order dynamic contribution also diverges, although only as $1/R$. This typically does not present a problem when the oscillator damping is dominated by nonradiative processes that overwhelm the shift.

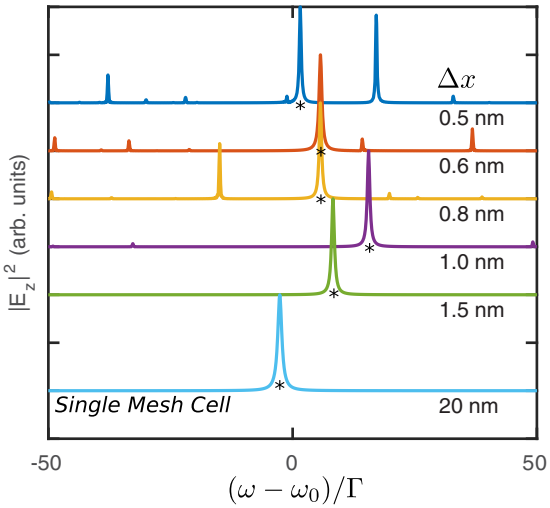

FIG. 2. Finite-difference time-domain simulations of the electric field intensity spectra generated by the sphere of LO material ($\omega_0 = 3.55 \times 10^{15}$ rad/s, $\mu = 690$ D, $\Gamma = 1 \times 10^{12}$ rad/s) with a 10-nm radius and permittivity given by Eq. (16) with $V = 4\pi R^3/3$, undergoing free decay in vacuum, with mesh sizes Δx labeled on the plot. The electric field is monitored 27 nm away from the sphere center. The asterisks mark the dipole-resonance peaks. The bottom spectrum is for a single-mesh cell LO with $\Delta x = 20$ nm and $V = \Delta x^3$, with its electric field monitored at the LO position. Each spectrum is calculated by taking the Fourier transform of the electric field after the excitation pulse has passed.

A sphere with this dielectric response function is defined and its response simulated in the FDTD solver. The resulting spectra of the decaying fields generated after impulsive excitation are shown in Fig. 2 for different mesh sizes. The sphere has a radius $R = 10$ nm, $\omega_0 = 3.55 \times 10^{15}$ rad/s, $\mu = 690$ D, and $V = 4\pi R^3/3$. In these simulations, the center of the sphere coincides with the E_z field location of one Yee cell. Note first that the relatively broad and resolved peak near ω_0, labeled by markers in all of these spectra, corresponds to the dipole response of this LO sphere. For it to accurately and usefully mimic the pointlike LO, ideally its frequency shift should be zero, its linewidth should be $\Gamma = \omega^3\mu^2\sqrt{\epsilon_B}/(3\pi\epsilon_0 c^3\hbar) = 1 \times 10^{12}$ rad/s, and there should be no other nearby resonant peaks. This mode's normalized shift and linewidth are plotted in Fig. 3. Although the shift appears to be converging to some value at small mesh sizes, the linewidth is still ill-behaved at the mesh sizes used in this study, and there are numerous spurious modes within a few linewidths of the main resonance, even at mesh sizes below 2 nm. We believe that these spurious resonances are numerical artifacts associated with the negative, undamped dielectric response function [shown in Fig. 1(a)] and the discrete cubic

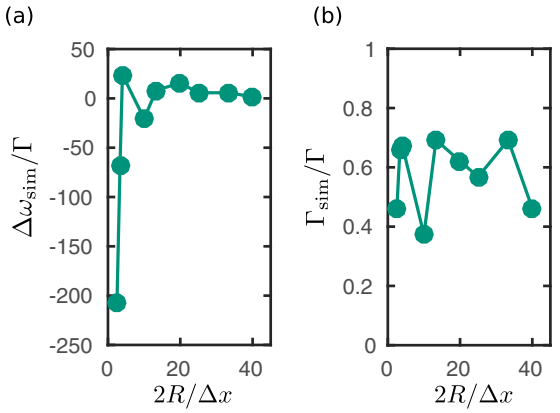

FIG. 3. FDTD simulation results for an LO material sphere freely decaying in vacuum with $R = 10$ nm, $\omega_0 = 3.55 \times 10^{15}$ rad/s, $\mu = 690$ D, and permittivity given by Eq. (16) with $\zeta = \sqrt{12/15}$, for different mesh sizes Δx. The simulated (a) frequency shift $\Delta\omega_{\rm sim}$ and (b) decay rate $\Gamma_{\rm sim}$ are both normalized to Γ. The volume V in Eq. (16) is set to $4\pi R^3/3$. The smallest five mesh sizes (rightmost data points in each plot) correspond to the resonant peaks marked by the asterisks in the upper five spectra in Fig. 2.

meshing. True higher-order resonance modes of ideal spheres with this response function exist [based on Mie scattering spectra shown in Fig. 1(b)] but they appear at frequencies well outside the spectral window shown in Fig. 2 for the $R = 10$-nm sphere. Given the important role that spherical symmetry plays in ensuring that the lowest-order real term in $\mathbf{G}_0(\mathbf{r},\mathbf{r}')$ results in a size-independent contribution to the internal field of the sphere, $-\frac{1}{3\epsilon_0\epsilon_{\rm B}(r_0)}\mathbf{P}_{\rm LO}(\mathbf{r})$, it is perhaps not surprising that it seems practically impossible to use FDTD in its nominal formulation to mimic a pointlike LO using a finite size sphere with reasonable computational resources.

C. Single mesh cell implementation of a "bulk" LO dielectric response function

Given that the issues associated with implementing a LO as a finite size sphere arise due to its meshing over many points, one possible remedy is to implement the LO on a single grid point. Remarkably, we find that if only a single grid point of one mesh cell is defined with the dielectric function [Eq. (16)] obtained from the Mie scattering simulations (something that makes no obvious sense in the FDTD formulation), the calculated decay spectrum is free of spurious modes and its linewidth is within a percent of the correct value. (See the bottom curve in Fig. 2.) Here the LO material is modified to cover only one field component of the Yee cell, as illustrated in Fig. 4(a), and the sphere volume V in Eq. (16) is set to match the Yee-cell volume ($V = \Delta x^3, R = [3/(4\pi)]^{1/3}\Delta x$).

This observation suggests it may be practical to implement pointlike LO objects in nanophotonic FDTD simulations. The background dielectric texture in such simulations will in general dictate the mesh size required for the macroscopic scattered fields $\mathbf{E}_{\rm B}$ to converge, and hence the volume of the single-cell LO materials one might want to include in the full scattering problem. Figure 4(b) shows the resonant frequency (open downward triangles) and linewidth (open circles) for a pointlike LO in vacuum ($\omega_0 = 3.55 \times 10^{15}$ rad/s, $\mu = 30.8$ D, $\Gamma = 2 \times 10^9$ rad/s, $V = \Delta x^3, R = [3/(4\pi)]^{1/3}\Delta x$) as a function of the mesh cell dimension, again using the dielectric function from Eq. (16) with the sphere volume V in the LO material set to match the Yee-cell volume ($V = \Delta x^3$). While the linewidth always remains within 5% of its nominal value, the resonant frequency is still systematically shifted from the correct value, with the magnitude of the shift increasing with decreasing cell size. For optical frequencies, this error in resonant frequency is greater than a linewidth even for mesh sizes as large as ~40 nm, and it is greater than 24 linewidths for mesh sizes less than 2 nm.

The residual shift of the single cell LO is reduced below a linewidth, to numerical noise, when $\zeta = 1.15$ is applied to the dielectric function in Eq. (16) instead of $\zeta = \sqrt{12/15}$,

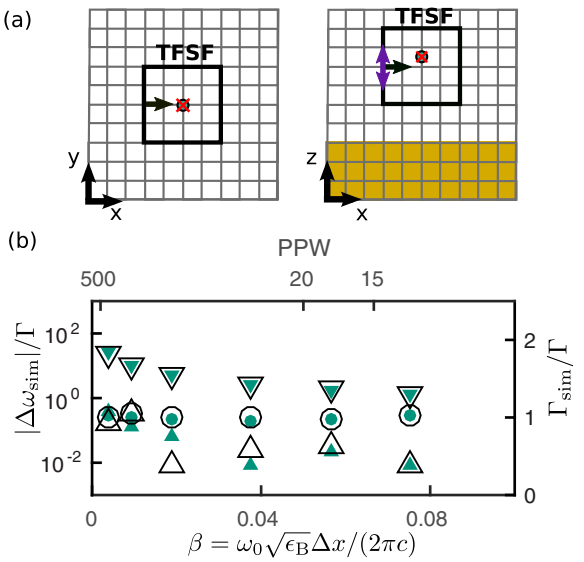

FIG. 4. (a) Layout used for three-dimensional FDTD simulations with background dielectric permittivity $\epsilon_{\rm B}$ (white), plotted in the $x-y$ plane (left) and $x-z$ plane (right). The edges of the Yee cells are indicated by the light-gray grid lines. The oscillator material (circle) is placed on a Yee-cell E_z field location, which is offset by half a mesh step in $\hat{\mathbf{z}}$ from the Yee-cell corner. The field at the E_z location is directly monitored by a detector (red cross). A total-field scattered-field (TFSF) source generates plane waves polarized in $\hat{\mathbf{z}}$ (double arrow in right schematic) traveling in the direction indicated by the black arrow, and only allows scattered fields to exist outside of it. The right schematic shows a gold half-space that spans the $x-y$ plane that is introduced in some inhomogeneous environment simulations. (b) FDTD simulation results for the free decay of a single Yee-cell LO material with $V = \Delta x^3$ (open empty markers) and LO plugin material (closed colored markers) in vacuum with resonance frequency $\omega_0 = 3.55 \times 10^{15}$ rad/s and dipole strength $\mu = 30.8$ D ($\Gamma = 2 \times 10^9$ rad/s from Fermi's golden rule). The simulation layout in (a) is implemented, without the gold half-space. On the left axis, the downward and upward triangles plot the magnitude of the simulated frequency shift relative to ω_0, $\Delta\omega_{\rm sim}$, normalized by Γ, for LOs with $\zeta = \sqrt{12/15}$ and $\zeta = 1.15$, respectively. They are plotted as a function of $\beta(\Delta x)$ (bottom axis), which is the mesh size expressed as a fraction of the wavelength in $\epsilon_{\rm B}$ and as a function of parts-per-wavelength (PPW), $1/\beta(\Delta x)$ (top axis). The simulated decay rates normalized by Γ are also plotted (circles, right axis), for the original LO material and the plugin material, using $\zeta = \sqrt{12/15}$.

as shown by the open upward triangles in Fig. 4(b), and the linewidth is maintained within 5% of its nominal value (not shown). From the above derivation of the effective LO dielectric function for the bulk sphere, the physical origin of this ζ factor must be associated with subtleties in how the FDTD solver evaluates what is effectively the average field over the single Yee cell where the LO is defined [24].

D. Alternate formulation of single-mesh cell dipole in FDTD

In the single Yee-cell LO implementation, the LO material effectively acts like a reactive point-dipole source, where the self-field generated at the LO location is dependent on its dipole moment. To deal with the residual shift associated with the average self-field over the Yee cell more directly, while at the same time shedding light on why this single-cell LO material works as well as it does, we use Lumerical's user-defined-material plugin tool, which allows one to create a material with a customized dipole moment response written in C^{++} code. In this "hands-on" approach, the plugin code is called at each time step to calculate the electric field based on the inputs fed to the code and the polarization density calculated within it. The plugin tool is most often used to model the nonlinear response of materials by defining *macroscopic* nonlinear susceptibilities in regions of space that are subdivided into many Yee cells [25,26].

As demonstrated below, if the polarization density of a "plugin material" is defined on a single cell, and derived based on a pointlike LO equation of motion, the FDTD algorithm faithfully evaluates the correct *microscopic* fields generated by the pointlike dipole, at cells located a few mesh points from the cell containing the plugin material. This is not so surprising, given the fact that, as noted in the Introduction, the imaginary part of the Green's function at points within some macroscopic dielectric environment can be obtained by using a "soft-point-dipole" source in FDTD, which allows all incident fields to pass through the source without scattering. For all intents and purposes, the "soft-point-dipole" source used in the evaluation of Green's functions in FDTD is a user-defined plugin that generates a fixed, nonresponsive oscillating polarization density within a single cell, *independent of any fields at that location*.

A pointlike LO plugin material is defined within a single Yee cell at one of the three locations where the electric fields are evaluated. The polarization density is taken to be $\mathbf{P}(t) = \mathbf{p}(t)/\Delta x^3$, where $\mathbf{p}(t)$ is the dipole moment, and the response is calculated in the C^{++} code using the following equation of motion:

$$\ddot{\mathbf{p}}(t) + \omega_0^2 \mathbf{p}(t) = \frac{2\omega_0 \mu^2}{\hbar} \mathbf{E}_{\rm tot}(t). \tag{18}$$

In the above equation, $\mathbf{E}_{\rm tot}(t)$ is the total electric field at the oscillator generated by the FDTD engine, which includes applied fields from external sources $\mathbf{E}_{\rm ext}(t)$, the self-field generated by the oscillator $\mathbf{E}_{\rm LO}(t)$, and scattered field $\mathbf{E}_{\rm scatt}(t)$. The equation of motion is reformulated in terms of the polarization density and the electric field at discrete time steps, and the dipole moment update is numerically estimated in the plugin code using values stored at previous time steps. In simulations with this plugin material, the divergent self-field contribution associated with $\mathbf{E}_{\rm LO}(t)$ can be subtracted "by hand" from the $\mathbf{E}_{\rm tot}(t)$ field supplied by the FDTD solver. Based on the analysis and results above, an obvious choice for estimating the field that has to be subtracted would be the inverse Fourier transform of the second term on the right-hand side of Eq. (14). Assuming the ω^2 term can be well-approximated by ω_0^2, the time-domain expression for the divergent field to be subtracted within the plugin from the total field provided to the plugin by the FDTD engine is then

$$\mathbf{E}_{\rm LO}^{\rm div}(t) = -[1 + f(\Delta x)]\mathbf{p}(t)/[3\epsilon_0 \epsilon_{\rm B}(\mathbf{r}_0)\Delta x^3], \tag{19}$$

where

$$f(\Delta x) = -[3/(4\pi)]^{2/3}(\zeta \omega_0 \Delta x \sqrt{\epsilon_{\rm B}}/c)^2. \tag{20}$$

When this LO plugin is simulated in vacuum with the divergent self-field taken as above with $\zeta = \sqrt{12/15}$, using the same dipole parameters ($\omega_0 = 3.55 \times 10^{15}$ rad/s, $\mu = 30.8$ D) and simulation parameters, as discussed above for the original Lorentz material, the resulting resonant frequency and linewidth are plotted in Fig. 4(b) as closed downward triangles and circles, respectively. They are essentially the same as what is obtained using the Lorentz-Lorenz dielectric function to define a single-cell LO material.

The residual shifts for the LO plugin are also reduced to below a linewidth when $\zeta = 1.15$, as shown in Fig. 4(b) (closed upward triangles), and linewidths are maintained within 5% of the nominal value (not shown). The ζ factor was originally associated with subtle details of the nonuniform depolarization field within the sphere. In this single-cell FDTD approach, there is no direct connection to this macroscopic interpretation, but the fact that the exact same, nontrivial function of the cube volume agrees so well with the spherical result indicates that the FDTD algorithm effectively generates a response closely associated with the average self-field over the cube-shaped Yee-cell volume. A future manuscript will detail a "proof" of this fact using an "analytic" solution of the FDTD algorithm that assumes the field calculated several mesh points away from the single cell containing the LO polarization are the exact dipole fields and works backwards to evaluate what the algorithm generates for the field at the impurity cell itself. For the present purposes it suffices to summarize the results of this ζ optimization problem for the single Yee-cell implementation.

The optimization procedure involves fitting the Fourier transform of the divergent field expression in Eq. (19),

$$\widetilde{\mathbf{E}}_{\rm LO}^{\rm div}(\omega) = -[1 + f(\Delta x)]\widetilde{\mathbf{p}}(\omega)/[3\epsilon_0 \epsilon_{\rm B}(\mathbf{r}_0)\Delta x^3], \tag{21}$$

to the continuous-wave (CW) self-field generated by a soft point source simulated with FDTD methods, to extract an estimate of the unknown parameter ζ in $f(\Delta x)$. The simulation layout is almost the same as in Fig. 4(a), except the Lorentz material is replaced by the point source polarized in $\hat{\mathbf{z}}$ and the total-field scattered-field source is removed. The soft point source has dipole moment $p_{\rm s}(t) = p_0 f(t)$, with $f(t) = \sin[-\omega_0(t - t_0)]\exp[-(t - t_0)^2/(2\sigma^2)]$. The normalized CW field amplitude $\widetilde{\mathbf{E}}_{\rm CW}(\mathbf{r_0},\omega)/p_0$ is extracted by taking the fast Fourier transform (FFT) of the monitored electric field $\mathbf{E}_{\rm s}(t)$ and dividing it by the FFT of $p_{\rm s}(t)$. Figure 5 plots the normalized FDTD results $\mathrm{Re}[\widetilde{\mathbf{E}}_{\rm CW}(\mathbf{r_0},\beta)/p_0]\Delta x^3$ (points) and the best-fit model function $\widetilde{\mathbf{E}}_{\rm LO}^{\rm div}(\beta)/\widetilde{\mathbf{p}}(\omega_0)\Delta x^3$ (solid lines),

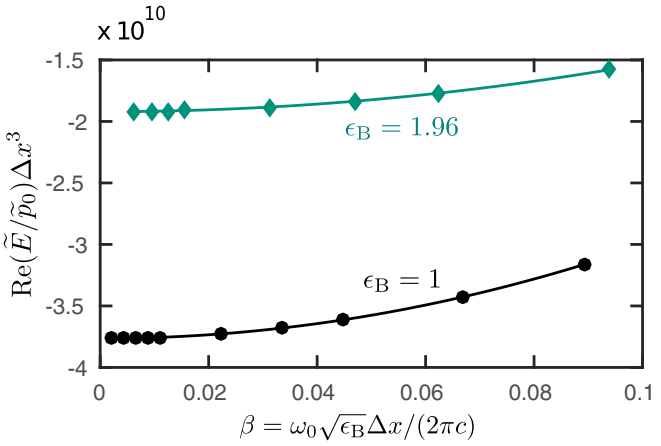

FIG. 5. The real part of normalized harmonic self-field found by FDTD simulations multiplied by the mesh cell volume Δx^3, $\widetilde{\mathbf{E}}_{\mathrm{CW}}(\mathbf{r_0},\beta)/p_0\Delta x^3$, is plotted for simulations with $\epsilon_B = 1$ (circles) and $\epsilon_B = 1.96$ (diamonds) as a function of $\beta(\Delta x)$. The real part of the normalized harmonic self-field predicted with our model $\widetilde{\mathbf{E}}^{\mathrm{div}}_{\mathrm{LO}}(\beta)/\widetilde{\mathbf{p}}(\omega_0)\Delta x^3$, with the best-fit values $\zeta_1 = 1.149\,3 \pm 0.000\,3$ (black line) and $\zeta_2 = 1.152\,1 \pm 0.000\,6$ (light line), is plotted for calculations with $\epsilon_B = 1$ and $\epsilon_B = 1.96$ (refractive index $n = 1.4$), respectively.

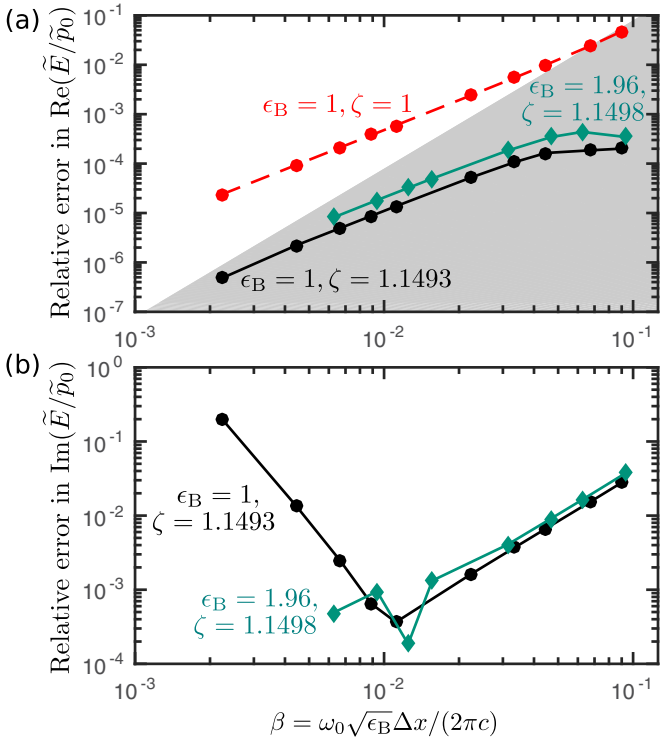

FIG. 6. (a) Relative error magnitude between our model, $\widetilde{\mathbf{E}}^{\mathrm{div}}_{\mathrm{LO}}(\beta)/\widetilde{\mathbf{p}}(\omega_0)\Delta x^3$, and the FDTD results, $\mathrm{Re}[\widetilde{\mathbf{E}}_{\mathrm{CW}}(\mathbf{r_0},\beta)/p_0]$, for the simulations in Fig. 5, plotted as a function of $\beta = \omega_0\sqrt{\epsilon_B}\Delta x/(2\pi c)$. Best-fit values $\zeta_1 = 1.149\,3$ and $\zeta_2 = 1.149\,8$, applied to $f(\Delta x)$ [Eq. (20)] for simulations with $\epsilon_B = 1$ (circles, solid black line) and $\epsilon_B = 1.96$ (diamonds, solid colored line), respectively. The red dashed line shows the relative error between the real part of the field amplitude averaged over one mesh cell ($\zeta = 1$) and $\mathrm{Re}[\widetilde{\mathbf{E}}_{\mathrm{CW}}(\mathbf{r_0},\beta)/p_0]$ for vacuum simulations ($\epsilon_B = 1.96$ results are not shown, as they are approximately the same). The shaded region indicates where the relative error causes frequency shifts of less than a linewidth in LO simulations. (b) Relative error magnitude between the predicted imaginary contribution, $(k_B)^3/(6\pi\epsilon_0\epsilon_B)$, and the FDTD results, $\mathrm{Im}[\widetilde{\mathbf{E}}_{\mathrm{CW}}(\mathbf{r_0},\beta)/p_0]$, for simulations with $\epsilon_B = 1$ (circles, solid black line) and $\epsilon_B = 1.96$ (diamonds, solid colored line).

where $\beta = \omega_0\sqrt{\epsilon_B}\Delta x/(2\pi c)$ is the mesh size expressed as a fraction of the wavelength in ϵ_B. The data is fit over $0.004 < \beta < 0.1$, a typical range to work within for FDTD simulations, and the resulting fit parameters are $\zeta_1 = 1.149\,3 \pm 0.000\,3$ and $\zeta_2 = 1.152\,1 \pm 0.000\,6$ for simulations with $\epsilon_B = 1$ (circles/black) and $\epsilon_B = 1.96$ (diamonds/light), respectively. A $\zeta = 1.15$ provides a good fit for simulations with background permittivities tested up to $\epsilon_B = 16$.

Despite the high accuracy of the model, a small net in-phase self-field contribution remains after subtraction, resulting in small frequency shifts in LO simulations. In general, the remaining frequency shift of a Lorentz oscillator in a homogeneous dielectric medium is approximately $-\Gamma/(8\pi^2\beta^3)$ times the relative error between $\mathrm{Re}[\widetilde{\mathbf{E}}_{\mathrm{CW}}(\mathbf{r_0},\beta)/p_0]$ and $\widetilde{\mathbf{E}}^{\mathrm{div}}_{\mathrm{LO}}(\beta)/\widetilde{\mathbf{p}}(\omega_0)$. The relative error is plotted in Fig. 6(a). The robustness of this model is reflected in both the excellent agreement with FDTD results and the small variation in the fit results for ζ, despite the fact that different simulation settings (like simulation volume, ω_0 and Δx) were sampled in each data set. For comparison, the relative error between the real part of the field amplitude averaged over one mesh cell and $\mathrm{Re}[\widetilde{\mathbf{E}}_{\mathrm{CW}}(\mathbf{r_0},\beta)/p_0]$ is plotted as the red dashed line in Fig. 6(a). The average field here is found by calculating the average of a point-dipole self-field over the cube volume, which, as it turns out, is well approximated by Eqs. (21) and (20) with $\zeta = 1$ [27]. The relative error of our model ($\zeta \simeq 1.15$) is between 40 to 200 times smaller than that from using the average over one mesh cell ($\zeta = 1$), over $0.004 < \beta < 0.08$. The shaded region in Fig. 6(a) shows where the magnitude of the relative error is less than $8\pi^2\beta^3$, which is where the resulting frequency shifts are approximately less than a linewidth. Shifts larger than a linewidth become particularly problematic in simulations of interactions between different emitters. This region is highly restrictive for small mesh sizes, where the absolute in-phase self-field is very large. Our model is sufficiently accurate to maintain frequency shifts less than a linewidth over $0.002 < \beta < 0.1$. This remains true when $\zeta = 1.15$ is applied to the model function, instead of the best-fit values, for simulations with background permittivities tested up to $\epsilon_B = 16$. For example, with $\lambda_0 = 531$ nm, $\mu = 30.8$ D (yielding $\Gamma = 2 \times 10^9$ rad/s), and a mesh size of 2 nm, the oscillator frequency is shifted by 0.31Γ, due to the relative error of -1.5×10^{-6} in the in-phase self-field calculation. In contrast, the model involving the integration over one mesh cell ($\zeta = 1$) results in shifts larger than a linewidth for $\beta < 0.06$. For example, with this $\zeta = 1$ relative error of 6.67×10^{-5}, the shift of the LO frequency is 15.8Γ.

The imaginary part of the GF at the point dipole is finite analytically and well behaved numerically, and does not require special modeling. The relative error between the predicted function for $(k_B)^3/(6\pi\epsilon_0\epsilon_B)$ and the FDTD results is plotted in Fig. 6(b). For $0.005 < \beta < 0.1$, the relative error remains below 4%, which is sufficiently low for a wide

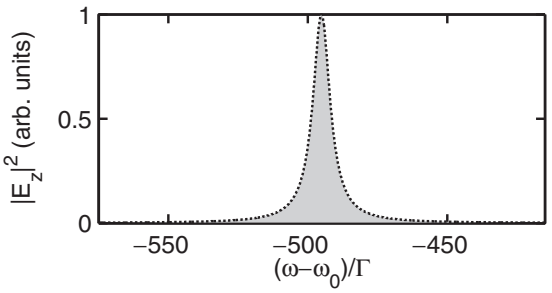

FIG. 7. The electric field intensity spectrum of a Lorentz oscillator (LO) in free decay, located 9 nm off the surface of a gold half-space is plotted (shaded region). The LO is simulated with FDTD methods using a plugin material with resonance frequency $\omega_0 = 2.51 \times 10^{15}$ rad/s ($\lambda_0 = 750$ nm) and dipole strength $\mu = 51.9$ D ($\Gamma = 2 \times 10^9$ rad/s) and $\Delta x = 2$ nm, that applies $\mathbf{E}^{\text{div}}_{\text{LO}}(t)$ to correct for the divergent self-field contribution. The simulated spectrum is fit by a Lorentzian line shape (dotted line).

range of applications, including simulations of the spontaneous emission rate, which is proportional to $\text{Im}[\widetilde{\mathbf{E}}_{\text{CW}}(\mathbf{r_0},\beta)/p_0]$. For large β (>0.1), $\text{Im}[\widetilde{\mathbf{E}}_{\text{CW}}(\mathbf{r_0},\beta)/p_0]$ increases from the model value and demonstrates known convergence limitations of the second-order FDTD algorithm. At small β (<0.005), $\text{Im}[\widetilde{\mathbf{E}}_{\text{CW}}(\mathbf{r_0},\beta)/p_0]$ also deviates from the theoretical value. In this range, $\text{Re}[\widetilde{\mathbf{E}}_{\text{CW}}(\mathbf{r_0},\beta)/p_0] \gg \text{Im}[\widetilde{\mathbf{E}}_{\text{CW}}(\mathbf{r_0},\beta)/p_0]$; thus it is possible that $\text{Im}[\widetilde{\mathbf{E}}_{\text{CW}}(\mathbf{r_0},\beta)/p_0]$ is inaccurately extracted due to the numerical precision of this calculation.

III. EXAMPLE APPLICATION

We now demonstrate how the LO plugin with the higher-order self-field correction included can be used to accurately capture the influence of macroscopic dielectric texture on the pointlike dipole dynamics. A LO located 9 nm off the surface of a gold half-space, polarized perpendicular to the surface (in $\hat{\mathbf{z}}$), is simulated with $\lambda_0 = 750$ nm ($\omega_0 = 2.51 \times 10^{15}$ rad/s) and $\mu = 51.9$ D, such that $\Gamma = 2 \times 10^9$ rad/s. The gold half-space lies outside of the total-field scattered-field (TFSF) source that excites the LO with a weak pulse, as illustrated in Fig. 4(a). A uniform mesh with $\Delta x = 2$ nm is applied within a 40 nm $\times$ 40 nm $\times$ 40 nm box surrounding the LO, and the mesh size is increased nonuniformly outside of the box. A time step of $\Delta t = 1.5 \times 10^{-3}$ fs is applied. The gold half-space is described by a Drude model $\epsilon_{\text{gold}} = 1 - \omega_p^2/(\omega^2 - i\omega\gamma)$, where $\omega_p = 1.26 \times 10^{16}$ rad/s and $\gamma = 1.41 \times 10^{14}$ rad/s. The decay spectrum is plotted in Fig. 7 and has a Lorentzian line shape, with a decay rate of 7.25Γ and total frequency shift of -495Γ. These are both consistent with the results calculated analytically[16]. The enhanced decay rate indicates that the local density of states is strongly modified at the oscillator. The frequency shift is dominated by scattering-induced effects, and the remaining shift due to the in-phase self-field is negligible, owing to the small relative error of our model function. With only the first-order (mesh-size-independent) self-field contribution applied in the model, the frequency shift due to the inaccurate in-phase self-field field is -95Γ, such that the total shift is -590Γ.

For large scattering shifts, it is more appropriate to use a modified version of the improved plugin, in which the in-phase part of the self-field is calculated as a time derivative, rather than assuming the second time derivative is proportional to ω_0^2. However, for most practical problems, where the scattering shift is a small fraction of ω_0, the two approaches work equally well.

The self-consistent resonant scattering of a *set* of pointlike QEs in the weak excitation limit can therefore be obtained in FDTD by exciting with an external field a scattering region defined by $\epsilon_{\text{r}}(\mathbf{r},\omega) = \epsilon_{\text{B}}(\mathbf{r},\omega) + \sum_i \chi_{\text{LO}}(\mathbf{r}_i,\omega)$, where $\chi_{\text{LO}}(\mathbf{r}_i,\omega)$ contributions are either defined using the original Lorentz material or the plugin material, but only if the higher-order correction factor to the dipole's in-phase self-field is used [Eq. (19) for the plugin, and Eq. (16) for the single-cell LO material). This requires that there is only one LO per Yee cell and that all LOs are either located in nonlossy background materials, or a real cavity model is applied where ϵ_{B} at the emitter is real, which is then inside the lossy material [24,28,29]. While this "single-cell LO material" approach is the fastest and easiest, the plugin approach can work for any FDTD Maxwell-medium approach, so the problem we highlight and solve is not restricted to a particular type of FDTD solver.

IV. SUMMARY

A pedagogical approach was taken to first understand what dielectric function $\epsilon_{\text{r}}(\omega)$ is required for a finite-size sphere to mimic the response of a point LO. Resonant frequency shifts that appear in Mie scattering spectra provide insight into the physical nature of the average in-phase self-field generated by the sphere polarization density. The response of the LO sphere is defined by relating the total induced dipole moment to the applied field as

$$\begin{aligned}\mathbf{p}_{\text{LO}}(\omega) &= \epsilon_0\chi_{\text{LO}}\int_V \widetilde{\mathbf{E}}_{\text{LO}}(\omega,\mathbf{r})d\mathbf{r} = \epsilon_0\chi_{\text{LO}}\overline{\mathbf{E}}_{\text{LO}}(\omega)V \\ &\triangleq \epsilon_0\alpha(\omega)\overline{\mathbf{E}}_{\text{B}}(\omega),\end{aligned} \tag{22}$$

where $\overline{\mathbf{E}}_{\text{LO}}(\omega)$ and $\overline{\mathbf{E}}_{\text{B}}(\omega)$ are the average $\mathbf{E}_{\text{LO}}(\mathbf{r},\omega)$ inside the sphere and the applied field at the sphere, respectively, and

$$\alpha(\omega) \simeq \frac{\epsilon_0^{-1}}{\frac{1}{\epsilon_0 V(\epsilon_{\text{r}}-\epsilon_{\text{B}})} - \mathbf{n}\cdot[\text{Re}[\overline{\mathbf{g}}_{\text{LO}}] + \mathbf{G}_{\text{s}}(\mathbf{r_0},\mathbf{r_0})]\cdot\mathbf{n}}, \tag{23}$$

where $\mathbf{G}_{\text{s}}(\mathbf{r_0},\mathbf{r_0}) = i\,\text{Im}[\mathbf{G_0}(\mathbf{r_0},\mathbf{r_0})] + \mathbf{G}_{\text{scatt}}(\mathbf{r_0},\mathbf{r_0})$, and $\text{Re}[\overline{\mathbf{E}}_{\text{LO}}(\omega)] = \text{Re}[\overline{\mathbf{g}}_{\text{LO}}(\omega)]\cdot\mathbf{p}_{\text{LO}}(\omega)$ defines $\text{Re}[\overline{\mathbf{g}}_{\text{LO}}(\omega)]$. The $\alpha(\omega)$ in Eqs. (10) and (23) are equated to find $\epsilon_{\text{r}}(\omega)$ for the sphere.

The unwanted frequency shifts are reduced to a fraction of the resonant linewidth by determining an accurate expression for the sphere-size-dependent $\text{Re}[\overline{\mathbf{E}}_{\text{LO}}(\omega)]$ to account for nonuniformities in the polarization density inside the sphere, given $\overline{\mathbf{E}}_{\text{B}}(\omega)$. In determining this average field response function, two levels of corrections, beyond the uniform polarization density approximation, turn out to be crucial. They both go as R^2 and thus introduce an R^2 dependence to the total induced dipole moment of the sphere, which leads to a $1/R$ contribution to the polarization *density* within the sphere. This explains the counterintuitive result that the nonuniform polarization

TABLE I. Key self-field corrections for various LO implementations.

Implementation	Field approximation	Material definition	Results
Mie theory, sphere	Constant field, lowest -order approximation, $\mathbf{Re}[\overline{\mathbf{E}}_{\mathrm{LO}}] \simeq -\frac{1}{3\epsilon_0\epsilon_{\mathrm{B}}V}\mathbf{p}_{\mathrm{LO}}$	$\epsilon_r = \epsilon_{\mathrm{B}} + \frac{\alpha_0(\omega)/V}{1-\alpha_0(\omega)/(3\epsilon_{\mathrm{B}}V)}$	Unwanted frequency shifts: $\Delta\omega \approx 6$–10Γ, ▲ in Fig. 1(c)
	Constant field, higher -order correction, $\mathbf{Re}[\overline{\mathbf{E}}_{\mathrm{LO}}] \simeq -\frac{1}{3\epsilon_0\epsilon_{\mathrm{B}}V}\mathbf{p}_{\mathrm{LO}}[1-(k_{\mathrm{B}}R)^2]$	$\epsilon_r = \epsilon_{\mathrm{B}} + \frac{\alpha_0(\omega)/V}{1-\alpha_0(\omega)[1-(k_{\mathrm{B}}R)^2]/(3\epsilon_{\mathrm{B}}V)}$	Unwanted frequency shifts: $\Delta\omega \approx 0.5$–2.6Γ, ● in Fig. 1(c)
	Nonuniform field, $\mathbf{Re}[\overline{\mathbf{E}}_{\mathrm{LO}}] \simeq -\frac{1}{3\epsilon_0\epsilon_{\mathrm{B}}V}\mathbf{p}_{\mathrm{LO}}[1-(\zeta k_{\mathrm{B}}R)^2]$, $\zeta = \sqrt{12/15}$	$\epsilon_r = \epsilon_{\mathrm{B}} + \frac{\alpha_0(\omega)/V}{1-\alpha_0(\omega)[1-(\zeta k_{\mathrm{B}}R)^2]/(3\epsilon_{\mathrm{B}}V)}$	Sublinewidth frequency shifts: $\Delta\omega \sim 0.02-0.09\Gamma$ ● in Fig. 1(c)
FDTD, meshed sphere	$\zeta = \sqrt{12/15}$	$\epsilon_r = \epsilon_{\mathrm{B}} + \frac{\alpha_0(\omega)/V}{1-\alpha_0(\omega)[1-(\zeta k_{\mathrm{B}}R)^2]/(3\epsilon_{\mathrm{B}}V)}$	Very small mesh sizes required for converged frequency shift. Decay rates fail to converge, likely due spurious modes present due to meshing.
FDTD, single-cell Lorentz material[a]	$\zeta = \sqrt{12/15}$, $V = \Delta x^3 \triangleq 4\pi R^3/3$	$\epsilon_r = \epsilon_{\mathrm{B}} + \frac{\alpha_0(\omega)/V}{1-\alpha_0(\omega)[1-(\zeta k_{\mathrm{B}}R)^2]/(3\epsilon_{\mathrm{B}}V)}$	Unwanted frequency shifts: $\Delta\omega \approx 1$–26Γ, ▽ in Fig. 4(b)
	Same as above but with $\zeta = 1.15$[b]	Same as above	Sublinewidth frequency shifts: $\Delta\omega \approx 0.008$–$0.4\Gamma$, △ in Fig. 4(b)
FDTD, single-cell plugin material[c]	$\zeta = \sqrt{12/15}$, $V = \Delta x^3 \triangleq 4\pi R^3/3$, $\mathbf{E}^{\mathrm{div}}_{\mathrm{LO}}(t) \simeq -\frac{\mathbf{p}(t)}{3\epsilon_0\epsilon_{\mathrm{B}}V}[1-(\zeta k_{\mathrm{B}}R)^2]$	$\ddot{\mathbf{p}}(t) + \omega_0^2\mathbf{p}(t) = \frac{2\omega_0\mu^2}{\hbar}[\mathbf{E}_{\mathrm{tot}}(t) - \mathbf{E}^{\mathrm{div}}_{\mathrm{LO}}(t)]$	Unwanted frequency shifts: $\Delta\omega \approx 1$–26Γ, ▼ in Fig. 4(b)
	Same as above but with, $\zeta = 1.15$[b]	Same as above	Sublinewidth frequency shifts: $\Delta\omega \approx 0.009$–$0.16\Gamma$, ▲ in Fig. 4(b)

[a] Easy to implement. Works in linear regime only.
[b] The divergent self-field generated by a point "soft source" at the dipole location is well described by simply setting $\zeta = 1.15$.
[c] General approach, can be extended to nonlinear regime. Requires additional technical knowledge of how to implement a custom material response (plugin). Gives effectively the same results as the single-cell Lorentz material when the same ζ is applied.

density correction terms become increasingly important for determining the resonant frequency shift as the sphere size *decreases*, because this shift is proportional to the polarization *density*. A summary of the $\epsilon_{\mathrm{r}}(\omega)$ resulting from various choices of $\mathrm{Re}[\overline{\mathbf{E}}_{\mathrm{LO}}(\omega)]$ is given in Table I, where the frequency shifts are calculated from Mie theory.

The insight gained from this pedagogical study is extended to two practical implementations of pointlike LOs in FDTD, where the LO material is defined on a single mesh cell. At several mesh steps away, the field generated by the LO replicates the microscopic field generated by a point dipole, whereas at the LO location, the field is effectively an average over the mesh cell. The average field is modeled with the same function as the corrected $\mathrm{Re}[\overline{\mathbf{E}}_{\mathrm{LO}}(\omega)]$ found for the Lorentz sphere, however, with a slightly different prefactor. The single-cell FDTD results are also summarized in Table I for Lorentz materials and plugin materials implemented with the LO sphere prefactor and the cubic cell prefactor. While the Lorentz material approach is limited to the weak excitation limit, a material plugin approach shows promise for more general modeling of QEs in arbitrary environments.

ACKNOWLEDGMENTS

We gratefully acknowledge financial support from the Natural Sciences and Engineering Research Council, including the Silicon Electronic-Photonic Integrated Circuits (Si-EPIC) CREATE Program and the Quantum Electronic and Science and Technology (QuEST) Program.

APPENDIX A: SUMMARY OF ELECTRIC FIELD NOTATION

The electric fields discussed above are summarized in Table II. The electric fields are marked with tildes (e.g., $\widetilde{\mathbf{E}}$) when the complex amplitude of the field is in use. The complex amplitude and time-dependent field are related through $\mathbf{E}(t) = \mathrm{Re}[\widetilde{\mathbf{E}}(\mathbf{r_0},\omega)\exp(-i\omega t)]$. The same electric field notation is applied for both point and sphere LOs.

APPENDIX B: MIE SHIFT

The $\zeta = \sqrt{12/15}$ scaling factor required to minimize the shift in resonant frequency can be explained in two ways. Most directly, if the analytic result for the Mie sphere polarizability from Refs. [22] and [23] is evaluated on resonance (where $\epsilon_r \simeq -2\epsilon_B$), one gets

$$\alpha = \frac{1+\frac{1}{10}(k_{\mathrm{B}}R)^2}{-\frac{4}{15}(k_{\mathrm{B}}R)^2 - i\frac{\omega^3\sqrt{\epsilon_{\mathrm{B}}}}{6\pi c^3}}, \tag{B1}$$

TABLE II. Summary of electric field notation.

Field	Description
$\mathbf{E}_{\text{ext}}(\mathbf{r})$	External electric field at position $\mathbf{r}$
$\mathbf{E}_{\text{B}}(\mathbf{r})$	Field generated at $\mathbf{r}$ due to external electric field $\mathbf{E}_{\text{ext}}(\mathbf{r})$ incident on $\epsilon_{\text{B}}(\mathbf{r})$
$\overline{\mathbf{E}}_{\text{B}}$	Average $\mathbf{E}_{\text{B}}(\mathbf{r})$ inside a sphere LO
$\mathbf{E}_{\text{LO}}(\mathbf{r}_0)$	Electric self-field generated by the polarization density of an LO at its center, located at $\mathbf{r}_0$
$\overline{\mathbf{E}}_{\text{LO}}$	Average $\mathbf{E}_{\text{LO}}(\mathbf{r})$ inside a sphere LO
$\mathbf{E}_{\text{LO}}^{\text{div}}(\mathbf{r}_0)$	Contribution to $\mathbf{E}_{\text{LO}}(\mathbf{r}_0)$ that is divergent for small mesh volumes
$\mathbf{E}_{\text{scatt}}(\mathbf{r}_0)$	Electric field due to scattering of $\mathbf{E}_{\text{LO}}$ off textured $\epsilon_{\text{B}}(\mathbf{r})$ back to $\mathbf{r}_0$
$\mathbf{E}_{\text{tot}}(\mathbf{r}_0)$	Total electric field present at $\mathbf{r}_0$, $\mathbf{E}_{\text{tot}}(\mathbf{r}_0) = \mathbf{E}_{\text{LO}}(\mathbf{r}_0) + \mathbf{E}_{\text{scatt}}(\mathbf{r}_0) + \mathbf{E}_{\text{B}}(\mathbf{r}_0)$
$\mathbf{E}_{\text{s}}(\mathbf{r_0})$	Electric field monitored at the soft-point-dipole source in pulsed-excitation FDTD simulations
$\mathbf{E}_{\text{CW}}(\mathbf{r_0})$	Continuous-wave electric field generated by soft-dipole-point source in FDTD calculated by taking the FFT of $\mathbf{E}_{\text{s}}(\mathbf{r}_0, t)$ divided by the FFT of the soft source's dipole moment

whereas using the formulation in Sec. II B, the corresponding expression is

$$\alpha = \frac{1}{-\frac{1}{3}(\zeta k_{\text{B}} R)^2 - i\frac{\omega^3\sqrt{\epsilon_{\text{B}}}}{6\pi c^3}}. \tag{B2}$$

For these to be consistent to lowest order in powers of $k_{\text{B}}R$, $\zeta^2/3 = 4/15$, or $\zeta = \sqrt{12/15}$.

The deviation of ζ from unity, the value estimated in Sec. II B by ignoring the nonuniformity of the polarization density within the sphere, is subtle but crucial for estimating the average polarization density accurately enough to remove unphysical frequency shifts in the net response. This is ultimately because the contribution of this nonuniform polarization density to the net dipole moment of the object scales as the radius squared and so makes a divergent contribution to the average polarization density when dividing by the volume: it is the polarization *density* that is responsible for the frequency shift.

[1] N. Somaschi, V. Giesz, L. D. Santis, J. C. Loredo, M. P. Almeida, G. Hornecker, S. L. Portalupi, T. Grange, C. Anton, J. Demory, C. Gomez, I. Sagnes, N. D. Lanzillotti-Kimura, A. Lemaitre, A. Auffeves, A. G. White, L. Lanco, and P. Senellart, Nat. Photonics **10**, 340 (2016).

[2] O. Gazzano, S. Michaelis de Vasconcellos, C. Arnold, A. Nowak, E. Galopin, I. Sagnes, L. Lanco, A. Lemaitre, and P. Senellart, Nat. Commun. **4**, 1425 (2013).

[3] X. Ding, Y. He, Z.-C. Duan, N. Gregersen, M.-C. Chen, S. Unsleber, S. Maier, C. Schneider, M. Kamp, S. Höfling, C.-Y. Lu, and J.-W. Pan, Phys. Rev. Lett. **116**, 020401 (2016).

[4] M. Arcari, I. Söllner, A. Javadi, S. Lindskov Hansen, S. Mahmoodian, J. Liu, H. Thyrrestrup, E. H. Lee, J. D. Song, S. Stobbe, and P. Lodahl, Phys. Rev. Lett. **113**, 093603 (2014).

[5] K. H. Madsen, S. Ates, J. Liu, A. Javadi, S. M. Albrecht, I. Yeo, S. Stobbe, and P. Lodahl, Phys. Rev. B **90**, 155303 (2014).

[6] B. Lounis and W. E. Moerner, Nature (London) **407**, 491 (2000).

[7] R. W. Ziolkowski, J. M. Arnold, and D. M. Gogny, Phys. Rev. A **52**, 3082 (1995).

[8] G. Slavcheva, J. M. Arnold, I. Wallace, and R. W. Ziolkowski, Phys. Rev. A **66**, 063418 (2002).

[9] W. Forysiak, R. G. Flesch, J. V. Moloney, and E. M. Wright, Phys. Rev. Lett. **76**, 3695 (1996).

[10] S. Hughes, Phys. Rev. Lett. **81**, 3363 (1998).

[11] H. Takeda and S. John, Phys. Rev. A **83**, 053811 (2011).

[12] A. Deinega and T. Seideman, Phys. Rev. A **89**, 022501 (2014).

[13] P. T. Kristensen and S. Hughes, ACS Photonics **1**, 2 (2014).

[14] E. S. C. Ching, P. T. Leung, A. Maassen van den Brink, W. M. Suen, S. S. Tong, and K. Young, Rev. Mod. Phys. **70**, 1545 (1998).

[15] M. Wubs, L. G. Suttorp, and A. Lagendijk, Phys. Rev. A **70**, 053823 (2004).

[16] L. Novotny and B. Hecht, *Principles of Nano-Optics* (Cambridge University Press, Oxford, UK, 2006).

[17] M. Sukharev and S. A. Malinovskaya, Phys. Rev. A **86**, 043406 (2012).

[18] R. Puthumpally-Joseph, O. Atabek, M. Sukharev, and E. Charron, Phys. Rev. A **91**, 043835 (2015).

[19] C. M. Bowden and J. P. Dowling, Phys. Rev. A **47**, 1247 (1993).

[20] C. F. Bohren and D. R. Huffman, in *Absorption and Scattering of Light by Small Particles* (Wiley-VCH Verlag GmbH, 2007).

[21] C. Matzler, "Matlab functions for Mie scattering and absorption", Research Report No. 2002-11, Institut fur Angewandte Physik, University of Bern (2002).

[22] H. Kuwata, H. Tamaru, K. Esumi, and K. Miyano, Appl. Phys. Lett. **83**, 4625 (2003).

[23] M. Meier and A. Wokaun, Opt. Lett. **8**, 581 (1983).

[24] C. Van Vlack and S. Hughes, Opt. Lett. **37**, 2880 (2012).

[25] R. Sinha, M. Karabiyik, C. Al-Amin, P. K. Vabbina, D. O. Guney, and N. Pala, Sci. Rep. **5**, 9422 (2015).

[26] Y. Sivan, S. Rozenberg, A. Halstuch, and A. A. Ishaaya, Sci. Rep. **6**, 29010 (2016).

[27] O. J. F. Martin and N. B. Piller, Phys. Rev. E **58**, 3909 (1998).

[28] S. Scheel, L. Knöll, and D.-G. Welsch, Phys. Rev. A **60**, 4094 (1999).

[29] M. S. Tomaš, Phys. Rev. A **63**, 053811 (2001).